JACS
JOURNAL OF THE AMERICAN CHEMICAL SOCIETY

Article

pubs.acs.org/JACS

The Coupling between Stability and Ion Pair Formation in Magnesium Electrolytes from First-Principles Quantum Mechanics and Classical Molecular Dynamics

Nav Nidhi Rajput,[†,§] Xiaohui Qu,[†,§] Niya Sa,[‡] Anthony K. Burrell,[‡] and Kristin A. Persson*[,†]

[†]Environmental Energy Technology Division, Lawrence Berkeley National Laboratory, Berkeley, California 94720, United States
[‡]Chemical Sciences & Engineering, Argonne National Laboratory, Lemont, Illinois 60439, United States

Supporting Information

ABSTRACT: In this work we uncover a novel effect between concentration dependent ion pair formation and anion stability at reducing potentials, e.g., at the metal anode. Through comprehensive calculations using both first-principles as well as well-benchmarked classical molecular dynamics over a matrix of electrolytes, covering solvents and salt anions with a broad range in chemistry, we elucidate systematic correlations between molecular level interactions and composite electrolyte properties, such as electrochemical stability, solvation structure, and dynamics. We find that Mg electrolytes are highly prone to ion pair formation, even at modest concentrations, for a wide range of solvents with different dielectric constants, which have implications for dynamics as well as charge transfer. Specifically, we observe that, at Mg metal potentials, the ion pair undergoes partial reduction at the Mg cation center ($Mg^{2+} \rightarrow Mg^{+}$), which competes with the charge transfer mechanism and can activate the anion to render it susceptible to decomposition. Specifically, $TFSI^{-}$ exhibits a significant bond weakening while paired with the transient, partially reduced Mg^{+}. In contrast, BH_4^{-} and BF_4^{-} are shown to be chemically stable in a reduced ion pair configuration. Furthermore, we observe that higher order glymes as well as DMSO improve the solubility of Mg salts, but only the longer glyme chains reduce the dynamics of the ions in solution. This information provides critical design metrics for future electrolytes as it elucidates a close connection between bulk solvation and cathodic stability as well as the dynamics of the salt.

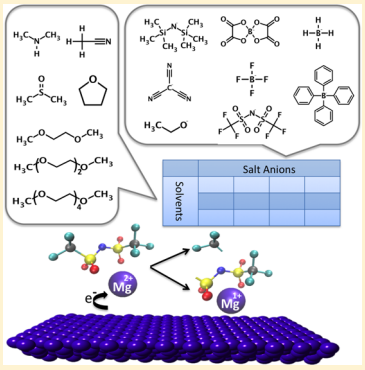

INTRODUCTION

To reduce the carbon imprint of our energy-dependent society it is essential to look for alternatives to fossil fuel. However, increasing the use of intermittent energy sources requires cheap, reliable storage to support a future sustainable energy grid and deployment. While the concept of Li-ion batteries was pioneered by Whittingham in the 1970s,[1,2] and demonstrated by Murphy et al. in 1980s,[3] it took almost 20 years to commercialize in the form of the Sony $LiCoO_2$/C rocking chair battery.[4] The development of Li-ion batteries enabled a breakthrough in electronic devices; however, despite extensive research during the last three decades, limited improvements have been achieved.[5] Li-ion batteries are still struggling with their limited performance, short lifetime and safety concerns. Thus, the focus is turning toward alternative, environmentally benign, higher energy density batteries such as lithium−air, lithium−sulfur and multivalent batteries. An approach to achieve energy density higher than the existing Li-ion batteries is to replace monovalent Li-ion by multivalent ions such as Mg, Ca. The ability of Mg batteries to provide much higher volumetric capacity, particularly on the anode side where the Mg metal can theoretically provide 3833 mA h/cc as compared to the Li counterpart graphite (~800 mA h/cc) at a lower cost makes the technology an attractive candidate for future batteries.[6] Despite several advantages the commercialization of Mg batteries faces numerous hurdles. Most Mg salts are incompatible with the traditional solvents used in Li-ion batteries; hence, Mg batteries suffer from the formation of a passive layer at the anode surface, blocking reversible Mg transport. Compared to Li-ion batteries the development of Mg batteries is still at a nascent stage and requires fundamental work to enhance our understanding of both the behavior and limitations of electrode materials as well as the electrolytes.

A future successful Mg battery requires an electrolyte with high ionic conductivity, wide electrochemical stability window, chemical compatibility with the electrode materials and low cost. Early studies of $Mg(ClO_4)_2$, and $Mg(BF_4)_2$ salts with organic solvents failed to enable reversible plating and striping of the Mg metal anode due to formation of a passive layer blocking the electrode interface.[7−9] Through the seminal work of Liebenow et al., it was established that Grignard-based ethereal solvents enable successful plating/striping of magnesium, however with a limited oxidative stability of ~1.5 V.[10] A series of electrolytes based on compounds such as amidomagnesium halides, organomagnesium compounds and magnesium organoborate in ethers such as tetrahydrofuran (THF) and primary

Received: January 29, 2015

DOI: 10.1021/jacs.5b01004
J. Am. Chem. Soc. XXXX, XXX, XXX−XXX

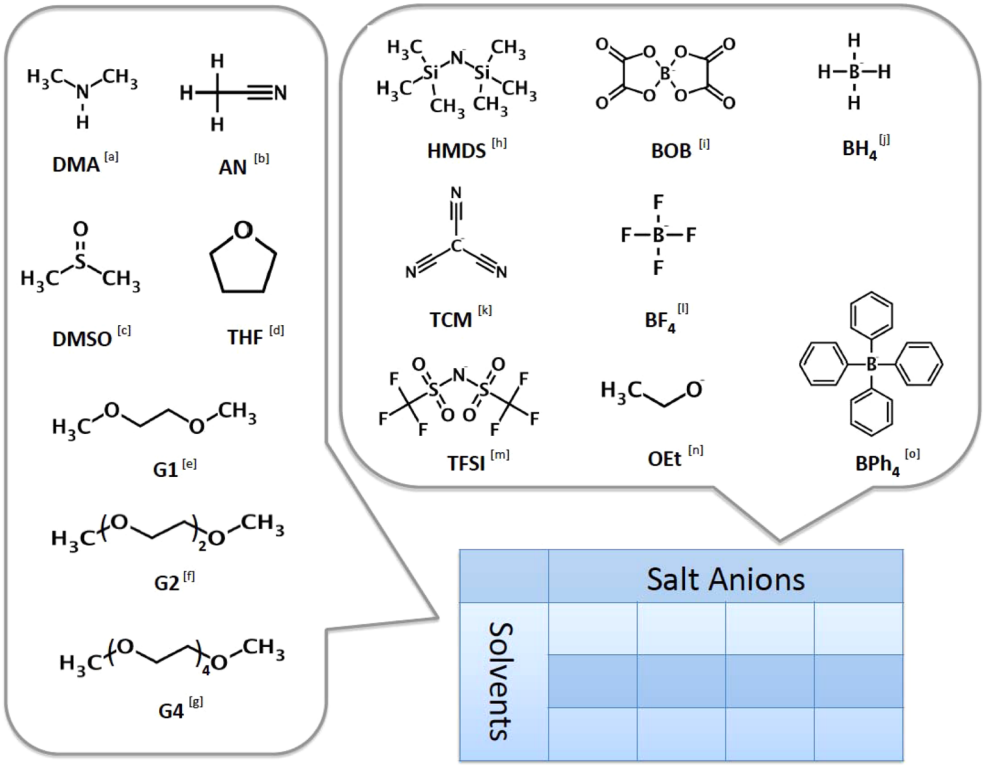

Figure 1. Solvent and salt anions of the electrolyte matrix. [a]Dimethylamine. [b]Acetonitrile. [c]Dimethyl sulfoxide. [d]Tetrahydrofuran. [e]Dimethoxyethane. [f]Diglyme. [g]Tetraglyme. [h]Bis(trimethylsilyl)amide. [i]Bis(malonato)borate. [j]Borohydride. [k]Tricyanomethanide. [l]Tetrafluoroborate. [m]Bis-(trifluoromethane)sulfonamide. [n]Ethoxide. [o]Tetraphenylborate.

amines were explored by researchers over the following years, however with limited stability and coloumbic efficiency.[10−13] In 2000 Aurbach demonstrated the first successful prototype rechargeable Mg battery with ∼60 W h/kg energy density, impressive cycle life (>3500 cycles) and negligible self-discharge.[14] However, the THF/Mg($AlCl_2BuEt_2$) electrolyte generation was limited by its ∼2.5 V electrochemical stability window due to the relatively weak Al−C bond which breaks with β−H elimination.[15] Doe et al. developed a family of Grignard-reagent free magnesium electrolytes (MACC) that demonstrated reversible plating/striping with ∼99% Coulombic efficiency and ∼3 V anodic stability on a platinum electrode.[16] On the other hand, Muldoon et al. demonstrated non-nucleophilic Hauser bases as electrolytes, hexamethyldisilazide magnesium chloride HMDSMgCl/$AlCl_3$ in THF and observed an excellent capacity of ∼1200 mAh/g in the first cycle but significant capacity fade in the second discharge.[17,18] Shao et al. studied the effect of the oxygen donor denticity of ethereal solvents with Mg(BH_4)$_2$.[19] These glyme-based solvents are chemically inert due to absence of functional groups and are known to demonstrate promising performance in Li-ion batteries as well as Mg batteries.[8,20−22] Some recent studies also show reversible Mg deposition and stripping in a electrolyte mixture of Mg(BH_4)$_2$ and $LiBH_4$ in glyme solvents and the effect of solvation structure on the stability of electrolytes.[19,23] An electrolyte solution based on Mg(TFSI)$_2$ in diglyme (G2) has recently demonstrated reversible electrochemical behavior, albeit with significant over potential, in a full cell configuration including a working Mg electrode.[24] Timothy et al. also reported reversible cycling of a Bi vs Mg cell using Mg(TFSI)$_2$ in acetonitrile (AN) as electrolyte.[25] However, the operation of this electrolyte at low potential is controversial as previous studies reports reduction of AN-based electrolytes at low potential.[8] On the other hand Tran et al. also observed reversible cycling and oxidation stability of ∼2.8 V of Mg(TFSI)$_2$ salt dissolved in AN. However, they did not observe plating of Mg and pointed out reduction of AN at ∼−0.2 V on stainless steel.[26]

In summary, despite several breakthroughs in the development of novel Mg electrolytes, improvements in electrochemical stability, compatibility with a variety of electrode materials, and ionic conductivity is needed. More importantly, there is a need for a comprehensive, fundamental understanding of the molecular-level interactions that govern the properties of multivalent electrolytes. Previous studies have shown that the solution solvation structure in these electrolytes is critical for reversible plating/stripping and formation of stable Mg complexes during stripping improves the columbic efficiency.[19,27] Specifically, in the case of Mg(TFSI)$_2$, which has been considered as one of the "holy grails" of magnesium batteries, there are several studies pointing to conflicting cathodic stability at Mg metal reduction potentials; hence, intriguing questions remain regarding the properties of Mg(TFSI)$_2$.[25,26,28] For example, it has been observed experimentally that the reduction peak shows strong dependence on the initial solute concentration.[29] However, very limited information is available in the literature on the local environment, particularly the degree of ion pairing, of these electrolytes. The concept of ion pair was first proposed by Arrhenius about a century ago with the definition of free ions-molecules or molecular fragments endowed with some electric charge.[30] Some previous studies have shown formation of ion pairs in Mg(TFSI)$_2$[31] and aqueous solutions of Mg(OAc)$_2$ and Mg(NO_3)$_2$.[32] This work aims to increase our knowledge of Mg electrolyte solvation structures to

DOI: 10.1021/jacs.5b01004
J. Am. Chem. Soc. XXXX, XXX, XXX−XXX

establish design metrics based on the intermolecular interactions that govern properties such as transport and stability.

METHODOLOGY

We employ a systematic approach, using an electrolyte matrix (Figure 1) consisting of 8 anions and 7 solvents to identify which chemical-structural features that correlate with desirable properties. The matrix was chosen to feature anions that have been previously applied in Mg electrolyte studies,[8,19,28,31] in addition to more uncommon ones,[17,18,33−35] to provide benchmarking as well as chemical breadth. Similarly, the solvents exhibit a range of dielectric constants, as well as cyclic and linear molecular structures. Using quantum mechanical calculations coupled with classical molecular dynamics (MD) simulations, the electrochemical stability window (ESW), solvation energy and decomposition path of electrolytes and their correlation with the intermolecular interactions and the resulting solvation structure were studied. Study of solvation structure provides insights of solution carrying ions, ion pairs and higher aggregates. While the concept of ion pairing is well established, there is no stringent quantitative definition. For example, an ion pair can be defined as the two oppositely charged ions in a solution which does not contribute to conductance.[36] In this work we considered the solvates formed in the solution as solvent separated ion pairs (SSIPs), contact ion pairs (CIPs) and aggregates (AGGs) if the average coordination number between the cation−anion is zero to one (SSIP), between one and two (CIP) or more than two (AGG), respectively in the first solvation shell. The solvation structure provides important insights with regards to the ion−ion and ion−solvent interactions, which in turn governs physical properties such as viscosity, conductivity, diffusion and vapor pressure.

Computational Details. *Quantum Chemistry Calculations.* To study the electrochemical stability of different multivalent salts in different solvents the electrochemical window as approximated by the ionization potential (IP) and electron affinity (EA) were computed for all combinations in the chosen electrolyte matrix (Figure 1). The IP and EA were calculated in the adiabatic approximation,[37] which takes into account the effect of structure relaxation on the reduction/oxidation potential, using the QChem software package[38,39] at the B3LYP 6-31++G** level.[40] The solvent effect was accounted for by an implicit solvent model: IEF-PCM,[41] where the solute−solvent interface was constructed using a van der Waals (vdW) surface defined from the Universal Force Field (UFF)[42] radii scaled by 1.1. Our previous work shows the details of workflow and benchmarked results using the same methodology.[43,44] Selected decomposition pathways were computed using quantum mechanical calculations for specific chosen electrolyte species. A vibrational frequency analysis was performed for every species to ensure that the relaxed molecular structure was obtained at the desirable stationary point. A minimum should have no imaginary frequency while a transition state should have one and only one imaginary frequency. By improving the structures iteratively, all final reported structures exhibit the desired number of imaginary frequencies. A counterpoise correction is employed for bond dissociation energy calculations to correct the basis set superposition error (BSSE).[45] All calculations are automated and carefully benchmarked by an in-house developed molecular high-throughput infrastructure.[44]

Molecular Dynamics Simulations. Classical molecular dynamics (MD) simulations were conducted on the electrolytes specified in Figure 1 using the GROMACS MD simulation package version 4.5.3.[46] General Amber force fields (GAFF) were used with the partial atomic charges derived by fitting the electrostatic potential surface generated from ab initio calculations for the optimized geometry.[47] The force field parameters were benchmarked against the experimental density and diffusivity and found to reproduce the experimental values adequately, the details of which are provided in the Supporting Information (SI), Table S1. The initial configurations were obtained by randomly packing the molecules in a cubic box with periodicity in the XYZ direction. We considered 0.4 M concentration for all systems with a box size of $4 \times 4 \times 4$ nm^3. Long-range electrostatic interactions were handled by the particle-mesh Ewald (PME) method with a cutoff distance of 1.2 nm and a grid spacing of 0.1 nm. A cutoff of 1.0 nm was used for Lennard−Jones interactions. An energy minimization was performed to relax the strained contacts in the initial configuration in two steps, first using steepest descent employing a convergence criterion of 1000 kcal/mol Å and then conjugated-gradient energy minimization scheme employing a convergence criterion of 10 kcal/mol Å. Isothermal−isobaric (NPT) simulations were performed for 2 ns to obtain the correct density of the systems using the Berendsen barostat.[48] Afterward, simulations were performed in the canonical ensemble (NVT) using the improved velocity-rescaling algorithm to mimic the weak coupling at the desired temperature with a time constant of 0.1 ps to equilibrate and sample properties of interest.[49,50] All systems were first melted at 400 K for 2 ns and subsequently annealed from 400 to 298 K in three steps for 2 ns. Structural and dynamical properties were obtained from a 10 ns MD simulation run with an integration time step of 0.5 fs in NVT ensemble. The simulation time was long enough to sample adequately the Fickian(diffusive) regime of all systems and the results were averaged over at least two independent realizations of the same system. We ran additional representative simulations with a larger box size ($8 \times 8 \times 8$ nm^3) and found no significant differences in the properties. Finally, the Einstein relation was used to measure the diffusion coefficient from the mean squared displacement of atoms. The resulting coefficient is fitted from a least-squares minimization for a straight line for a time period in the diffusion regime and then averaged over two independent realizations of the same system.

Experimental Details. *Materials and Electrolyte Preparation.* Magnesium bis(trifluoromethane sulfonyl)imide (99.5%, Solvionic, France) was dried in a vacuum oven overnight before use. G2 (Aldrich, anhydrous, 99.5%) solvent was pretreated with a molecular sieve (Aldrich, 3 Å beads, 4−8 mesh) and then added to the dried $Mg(TFSI)_2$. The as prepared electrolyte was then stirred overnight before use.

Characterization of the Diffusion Coefficient. A three electrode configuration composed of a Pt disk as working electrode (2 mm in diameter, CH instruments, Austin, TX) and Mg ribbon as counter and reference electrode (99.9% purity, Sigma-Aldrich) was applied to determine the diffusion coefficient of $Mg(TFSI)_2$ in G2. The chronocoulometry (CC) method was used to measure the diffusion coefficient of the Mg cations in the electrolyte. The potential at the working electrode was held at −0.5 V for 300 s allowing reduction of the Mg cations to reach at the electrode surface. The electrochemical characterization was carried by a multichannel potentiostat (Parstat MC, Princetion Applied Research, TN) under pure argon atmosphere in a glovebox. Integration of current density over time was obtained and plotted against the square root of time as shown in Figure S27. The diffusion coefficient was determined by fitting Q *versus* $t^{1/2}$ with eq 1 derived from the Cottrell equation;

$$Q = \frac{2nFAC_0D^{1/2}}{\pi^{1/2}}t^{1/2} + Q_{dl} + Q_{\text{ads}} \quad (1)$$

where n is the number of electrons for the reduction reaction occurred at the working electrode ($n = 2$); F is the Faraday constant; A is the electrode area (0.0314 cm^2), Q_{dl} is the capacitive charge and Q_{ads} is the charge contributed from the absorbed species.

Cyclic Voltammetry and Linear Sweep Voltammetry. Cyclic voltammetry (CV) and linear sweep voltammetry (LSV) was characterized based on a three-electrode configuration, with working electrode as a platinum disk (2 mm in diameter, CH instruments, Austin, TX), counter electrode and reference electrode as Mg ribbons (99.9% purity, Sigma-Aldrich). Potential was swept from −1 to +3 V vs Mg/Mg^{2+} with 25 mV/s as scan rate. Measurements were carried on a multichannel potentiostat (Parstat MC, Princetion Applied Research, TN) under pure argon atmosphere in a glovebox.

RESULTS AND DISCUSSION

1. Ionization Potential/Electron Affinity (ESW). Electrochemical stability is one of the key determinants of electrolytes; hence a detailed exploration is essential. It is assumed that a good candidate multivalent salt should contain an anion as well as a solvent that is tolerant to the operating voltage of the battery. In

DOI: 10.1021/jacs.5b01004
J. Am. Chem. Soc. XXXX, XXX, XXX−XXX

this work we focused on the stability of the anion, which sets the limit for many Mg battery electrolytes.[8,22,51,52] To obtain a first guide to the anion stability as a function of anion chemistry and structure, we calculated the electrochemical window of all the anions in the electrolyte matrix, within the implicit solvent model. While an implicit solvent model may not provide accurate quantitative results it has been found to provide the correct trends as to the stability of the salt components when compared within the same model.[37] The results are shown in Figure 2, set relative to the Mg^{2+}/Mg redox pair at 0.0 V. The electrochemical window is expressed by two properties: the IP and EA. The IP represents the energy penalty to oxidize an anion, while the EA is the energy gained for a reduced anion. In other words, the EA must be lower than the cathodic limit (0 V in Figure 2), while IP should be higher than the anodic limit (set by the operating voltage of the cathode). In this paper, all the IP/EAs are calculated by the energy gap between the final and initial state of the fully relaxed molecule at each charge state, respectively. We have also calculated the LUMOs of specific molecules of interest to analyze the nature of reduction; however, it should be noted that the LUMO is not used in the calculation of IP and EA. In Figure 2a, all the solvated anions except BOB^- have EA well below 0 V (cathodic limit) and are hence tentatively predicted to be stable against reduction, in their well-solvated form, at Mg metal potentials. Furthermore, all solvated anions, except $HMDS^-$ and OEt^-, are predicted to be stable against oxidation up to 2 V. The highest oxidation potentials are obtained for $TFSI^-$ and BF_4^-. To assess the reliability of the quantum chemistry calculations within the class of one salt and several different solvents, we compared the theoretical predictions of electrochemical stability in various solvents for the $TFSI^-$ anion with experimental measurements. Linear sweep voltammetry (see Experimental Details section for details) was employed to measure the anodic limit of the electrolyte, which correlates with the predicted IP of the anion—assuming that other components of the electrolyte (e.g., the solvent) are stable. The results are shown in Figure S1 and Table S2. Across all five solvents, the $Mg(TFSI)_2$ solution exhibits an anodic limit between 3.6 and 4.1 V as shown by LSV, while the theoretical predictions of IP range from 4.9–5.1 V depending on the solvent. The anodic stability of $Mg(BH_4)_2$/THF is predicted ~1.5 V lower than $Mg(TFSI)_2$, which should be compared to the corresponding 1.5–2 V lower experimental anodic stability. Similarly, $Mg(BF_4)_2$/AN is predicted to exhibit a ~2.5 V higher oxidation potential than $Mg(TFSI)_2$ which correlates with the 1.5 V increase in experimental anodic stability. Hence, we find a good correlation between the theoretical predictions and experimental measures which indicates that the computational procedure is adequate to predict at least the fundamental trend of the anion anodic stability.

Furthermore, we find that the solvent effect, approximated by the PCM model, only contributes to a small scatter of the anion IP/EA values. However, incorporation of explicit solvent molecules to the model system can capture more details of the solvent effects. For comparative purposes, we also calculated the IP/EA of $TFSI^-$ coordinated by one solvent molecule, in addition to the IEF-PCM model. This combined explicit-implicit solvent model calculation was carried out for 4 representative solvents: AN, G2, DMSO and THF. As shown in Table S2, the combined explicit-implicit model predicts slightly narrower electrochemical windows than the implicit solvent model, indicating that the implicit solvent currently used in this work is likely to overestimate the electrochemical stability of the salt anion. The largest error is found for $TFSI^-$ in G2, where the implicit solvent overestimates the IP by 0.55 eV while underestimating the EA by 0.03 eV. However, it should be noted that the trend of the implicit solvent model is qualitatively correct. For example, both the implicit solvent model and combined explicit-implicit solvent model predict $TFSI^-$ to be stable at Mg metal potentials. Also, the *relative* trend among different solvents is in good agreement between the two methods. As the purpose of this paper is to study relative chemical trends and correlations between electrolyte solvation and properties, such as stability, rather than calculating the absolute electrochemical windows, the implicit solvent model is deemed appropriate to provide an efficient while reasonably accurate approach.

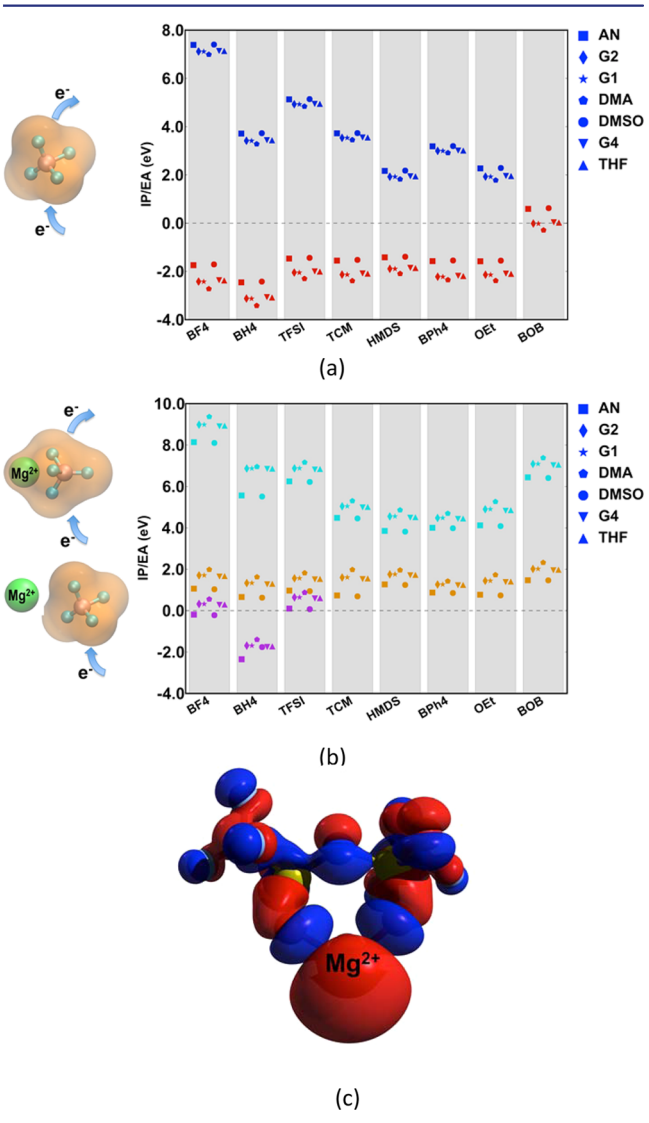

Figure 2. Calculated electrochemical windows (IP/EA) of different salt anions in different solvent dielectric media. All the values are reported *versus* Mg^{2+}/Mg, and the solvent effect is taken into account by the IEF-PCM model. All the solvents are listed in the legend and indicated by different symbols. (a) IP/EA of the well-solvated anion where red dots are EAs; blue dots are IPs. (b) IP/EA of the solvated $[Mg–Anion]^+$ ion pairs where orange dots are EAs; cyan dots are IPs and violet dots depict the EAs of the anions, constrained to accept the electron, for the $[Mg–Anion]^+$ ion pair. (c) The LUMO of an $[Mg^{2+}–TFSI^-]^+$ ion pair.

DOI: 10.1021/jacs.5b01004
J. Am. Chem. Soc. XXXX, XXX, XXX–XXX

Our calculation results are consistent with available trends known from experimental observations showing BH_4^-[19] based salts to be stable for Mg metal anode plating/stripping and $TFSI^-$ salts[28] at higher potentials. Similarly, our results indicate electrochemical stability of BF_4^- against direct reduction; however, previous studies have shown that BF_4^- is vulnerable to chemical decomposition.[8] However, interestingly, inconclusive evidence is reported on the stability of the $Mg(TFSI)_2$ salt at Mg metal potentials.[22] For example, while 0.3 M $Mg(TFSI)_2$ in G1/G2 was found to be compatible with Mg metal, a higher concentration of 0.5 M $Mg(TFSI)_2$ in G1/G2 demonstrated an unstable potential profile associated with possible passive film formation for the Mg stripping and deposition process.[28] To elucidate the reason for the change in stability with salt concentration for $Mg(TFSI)_2$, we turned our focus to the solvation structure of the electrolyte. Some lithium salts such as $LiBPh_4$, $LiCF_3CO_2$, LiBr, $LiNO_3$, $LiCF_3SO_3$ and $LiBF_4$ have demonstrated different degrees of ion pairing in solvents like glymes and AN.[53,54] Similar ion pairing has also been observed for Mg−TFSI in ionic liquid electrolytes and also in PEO at high concentrations.[55,56] Aqueous solutions of $Mg(ClO_4)_2$, $Mg(SO_4)_2$, $Mg(NO_3)_2$, $MgCl_2$ are also known to show ion pair formation at high concentrations (>2 M); however, $Mg(OAc)_2$ shows ion pair formation at lower concentrations (>1 M).[57,58] Previous experimental studies using X-ray absorption fine structures (XAFS) on Mg salts such as $Mg(AlCl_2EtBu)$/THF have observed the formation of complex salt-solvent structures $(Mg_2Cl_2THF_4)^{2+}$ in the solution.[59] Furthermore, the all phenyl complex (APC) type electrolytes exhibit a strong tendency for Mg complex formation.[60] Recently, it was shown that $Mg(TFSI)_2$/G2 exhibits a significant degree of ion pairing even at moderate concentrations such as 0.4 M.[61] Hence, it is a reasonable assumption that Mg salts are prone to ion pair formation, even at moderate concentrations and particularly in solvents such as ethers with low dielectric properties. While ion pair formation is known to negatively impact charge transfer[62,63] and conductivity,[64,65] very little is known about the effect of ionic association on the stability of multivalent electrolytes, particularly at Mg metal reduction potentials.

To investigate the impact of ion pair formation on the stability of the electrolyte, we calculated the IP/EA of the all the considered $[Mg−Anion]^+$ ion pairs in different dielectric media corresponding to different solvents. The results are shown in Figure 2b where it is evident that both the IP and EA are significantly elevated for the solvated ion pair compared to the well-solvated anion. It is intuitive that a strong interaction between the anion and the highly electropositive Mg^{2+} cation increases the tendency toward reduction as well as the penalty to oxidize the complex $[Mg−Anion]^+$ ion pair as a whole. To investigate the electronic structure of the reduced complex, we performed a natural bond orbital (NBO)[3] population analysis for one of the reduced ion pairs; the Mg−TFSI ion pair. The NBO result shows that the atomic charge and spin density on Mg is 0.88 and 0.89 respectively, for the reduced Mg−TFSI ion pair. Hence, the changes in atomic charge as well as the spin density clearly indicate that the electron-accepting component in the Mg−TFSI ion pair is the Mg^{2+} cation rather the $TFSI^-$ anion. This can be further elucidated from molecular orbital analysis. Figure 2c shows the lowest unoccupied molecular orbital (LUMO) of $[Mg^{2+}−TFSI^-]^+$. The majority LUMO of $[Mg^{2+}−TFSI^-]^+$ is associated with Mg^{2+}; therefore, Mg^{2+} is the most likely to reduce if an electron is added to the complex. Since the $Mg^+−TFSI^-$ ion pair carries an unpaired electron, we postulate that the complex is chemically active and transient. The complex can either further accept one more electron from the electrode (Mg metal in this case), corresponding to charge transfer ($Mg^+ \rightarrow Mg^0$), or undergo chemical decomposition. To confirm that the reduction of the Mg^{2+} cation in the ion pair is indeed the lowest reduced energy state of the complex, we calculated the EA by constraining the reduction to the anion for three anion pairs; $[Mg^{2+}−BH_4^-]^+$, $[Mg^{2+}−BF_4^-]^+$, $[Mg^{2+}−TFSI^-]^+$ (see Figure 2b), using the absolutely localized molecular orbitals (ALMO)[4] method. It was found that the *anion* EA in the ion pair is also elevated by presence of the Mg^{2+} cation, albeit not as much as the EA of the complex when allowing the Mg cation to reduce. From Figure 2b, we observe that the anion EAs for the three examined pairs are all very close to Mg metal potentials; however, given the qualitative nature of the PCM method, it is inconclusive whether the results indicate electrochemical instability or not. It is likely though, that there exist a strong correlation between ion pair formation and increased tendency toward reduction of the anion. This correlation between ion pair formation, which is explicitly dependent on the concentration and nature of the salt, and anion stability is a possible explanation for the discrepant results reported on the $TFSI^-$ stability in the literature. We emphasize that (1) the results presented are obtained using approximate, implicit solvent methods and some calculation error should be expected (as discussed previously in this section) and that (2) the reduction potential indicated by the EA may be preceded by a chemical decomposition of $[Mg^{1+}$-Anion] ion pair, which is investigated in the following section.

2. Decomposition of the Mg−TFSI Ion Pair. Our work indicates that an ion pair (e.g., $[Mg^{2+}−TFSI^-]^+$) is significantly easier to reduce than a well-solvated anion alone. There are two possibilities for the fate of reduced, transient Mg−TFSI ion pair: (1) Obtain one more electron from the electrode, which leads to Mg reduction and charge transfer to the Mg^0 state and leaves $TFSI^-$ unchanged. In other words, the $TFSI^-$ anion is stable in this situation. (2) Undergo chemical decomposition involving either anion and/or solvent, which will lead to irreversible reactions, electrolyte loss, and possible deposition of decomposition products on the Mg anode surface. To study the effect of ion pair formation on chemical stability, we calculated the bond dissociation energy (BDE) for the three anions, $TFSI^-$, BH_4^- and BF_4^- under different conditions corresponding to (1) a well-solvated anion, (2) a solvated ion pair with Mg^{2+}, and (3) a solvated ion pair with a reduced, transient Mg^+. While BH_4^-/BF_4^- exhibits only one unique bond (B−X), in $TFSI^-$ we examine all the noncyclic bonds: C−S, C−F and S−O. As shown in Figure 3 it was found that the BDEs in all three configurations for BH_4^- and BF_4^- exhibit similar trends. The ion pair association of the anion with the Mg^+ decreases the bond dissociation energy of B−H and B−F by 1.22 and 1.68 eV respectively. However, they are still as high as 3.03 and 5.80 eV respectively. In contrast, the cation-reduced Mg^+TFSI^- complex exhibits a dramatically decreased dissociation energy of the C−S bond from 2.41 eV to −0.85 eV. In other words, the association with Mg^+ causes the C−S bond breaking to change from an endothermic reaction to an exothermic reaction. The transition state is also successfully located and the barrier height is found to be as low as 0.02 eV. The extremely low barrier height and exothermic reaction enthalpy strongly indicate that the Mg^+TFSI^- complex is likely to rapidly decompose into the fragments CF_3 and $[CF_3SO_2NSO_2]$-Mg^0. As a precaution for the qualitative nature of implicit solvent models, we also calculated the BDEs using the combined explicit-

DOI: 10.1021/jacs.5b01004
J. Am. Chem. Soc. XXXX, XXX, XXX−XXX

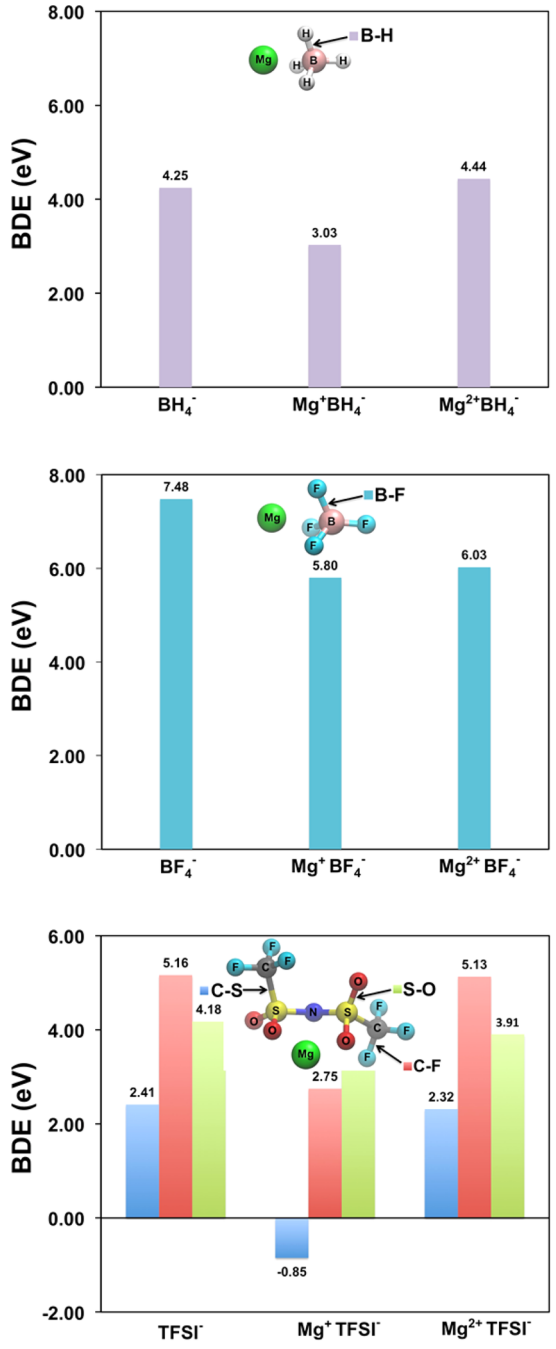

Figure 3. Bond dissociation energy (BDE) of BH_4^-, BF_4^-, and $TFSI^-$ in different chemical environments corresponding to well-solvated, Mg^+ ion paired and Mg^{2+} ion paired configurations in a PCM model.

implicit solvent model. As shown in Figure S2, the trend of implicit solvents model is well reproduced. Surprisingly, the dissociation of C−S bond in $TFSI^-$ is found to be more exothermic in combined explicit-implicit model than in implicit solvent model with a BDE at −1.84 eV, indicating that the actual decomposition tendency of the C−S bond in $TFSI^-$ could be even stronger under ion paired charge transfer conditions. As discussed above, this predicted chemical decomposition reaction will compete with further electrochemical reduction of the Mg cation followed by deposition (charge transfer) on the anode electrode. Thus, we predict $TFSI^-$ to be inherently electrochemically stable in its solvated form for a wide potential range, which is supported by its proposed use in Li systems.[66−68]

However, we also find that the electrochemical reduction of the $Mg^{2+}TFSI^-$ ion pair complex in solution activates $TFSI^-$ and renders it liable toward rapid chemical decomposition. Even at moderate concentrations such as 0.4 M, $Mg(TFSI)_2$ demonstrate a significant degree of ion pairing.[61] As a consequence, Mg^+-initiated decomposition is likely to affect the stability of $Mg(TFSI)_2$. Ha et al.[28] speculated that the change in over potential and film formation on the Mg metal anode with $Mg(TFSI)_2$ concentration was due to changes in conductivity with higher concentration; however, they found the conductivity higher for 0.5 M as compared to the 0.3 M solution. Hence, we suggest that the experimentally observed instability of 0.5 M $Mg(TFSI)_2$/G1/G2 may instead be a result of the increased ion pairing with higher concentrations, which in turn leads to a higher number of $TFSI^-$ anions being exposed to the transient Mg^+ radical and subsequent decomposition.[28] In agreement with experimental result, BF_4^- and BH_4^- are found to be stable even as ion pairs. Therefore, BH_4^- and BF_4^- are less prone to decomposition as compared to $TFSI^-$ in the electrolyte. It should be emphasized that the instability mechanism studied in this paper is only one decomposition path among many possibilities, particularly if impurities of the electrolyte are also considered. For example, an electrolyte predicted to be stable in one environment might be unstable due to water impurities and hydrolysis-mediated decomposition mechanisms.[69]

3. Solvation Structure and Ionic Association. Given the importance of solvation structure and possible ion pair formation for the stability of the salt anion, we studied the solvation structure of Mg salts for the various solvents considered in the electrolyte matrix using classical MD simulations. To investigate the local solvation structure, we computed the cation−anion, cation−solvent and cation−cation radial distribution function (RDF) for three representative systems $Mg(TFSI)_2$, $Mg(BH_4)_2$ and $Mg(BF_4)_2$ in the seven solvents considered in the electrolyte matrix (see Figure 1). For the sake of comparison we studied all systems at 0.4 M concentration, even though, e.g., $Mg(BH_4)_2$ is known to exhibit very low solubility (below 0.4 M) in many solvents.[19] The solvates formed in the electrolyte mixtures are divided in to three categories: (1) solvent-separated ion pairs (SSIPs), (2) contact ion pairs (CIPs) and (3) aggregates (AGGs) for zero to one, one to two, and two or more than two anions coordinated around Mg^{2+} respectively.[53] The RDFs and snapshots of the 21 systems studied are provided in the Supporting Information (see Figure S3−S23). For $Mg(TFSI)_2$ salt we computed RDF between Mg−O(TFSI), Mg−N(TFSI), Mg−N(AN, DMA), Mg−O(G1, G2, G4, DMSO, THF) and Mg−Mg (Figure S3−S9). We observed that the first peak in the solvation shell originates from the oxygen atoms of TFSI and O donor solvents G1, G2, G4, DMSO, THF at ∼2.1 Å, which indicates a strong interaction between Mg^{2+} ions and the oxygen of $TFSI^-$ and solvent molecules. For N chelating solvents, AN and DMA, the Mg−N peak is observed at ∼2.2 Å. However, the peak height of Mg−O (G1, G2, G4, DMSO) and Mg−N (AN, DMA) varies for different solvent depending upon the strength of the interaction with Mg^{2+}. For example, the strong and sharp peak of Mg−O(TFSI) as compared to Mg−N(AN, DMA) indicates a stronger interaction of $TFSI^-$ with Mg^{2+} than the N chelating solvents. For O chelating solvents (G1, G2, G4, DMSO, THF) the Mg−O (solvent) peak is much smaller as compared to the Mg−O(TFSI) peak in case of G1 and THF, which results in formation of AGGs in G1 and THF. In G2, the Mg−O(solvent) peak is slightly smaller than the Mg−O(TFSI) peak which results in formation of CIPs in the solution, On the

DOI: 10.1021/jacs.5b01004
J. Am. Chem. Soc. XXXX, XXX, XXX−XXX

other hand Mg−O(solvent) peak is larger than Mg−O(TFSI) in G4 and DMSO resulting in SSIPs in the solution. The peak from the Mg−N(TFSI) interaction is observed at a larger distance of ∼4.1 Å for all solvents due to steric hindrance from two large sulfonyl groups of the $TFSI^-$ anion. The features of Mg−Mg peaks vary significantly for different solvents. The Mg−Mg peak is negligible in case of G2, G4 and DMSO indicating very weak interactions between Mg^{2+} ions, which result in highly solvated ions in the solution. The snapshots in Figure S3−S19 indicate formation of clusters in AN, DMA, G1 and THF and more solvated ions in G2, G4 and DMSO. For the $Mg(BF_4)_2$ salt we computed RDF between Mg−F(BF_4), Mg−B(BF_4), Mg−N(AN, DMA), Mg−O(G1, G2, G4, DMSO, THF) and Mg−Mg (Figure S10−S16). In the $Mg(BF_4)_2$ electrolytes the first peak in the solvation structure is observed from Mg−F(BF_4) at ∼2.1 Å followed by a sharp peak from Mg−B(BF_4) at ∼3.5 Å with a small kink at 2.8 Å. Similar to $Mg(TFSI)_2$, the difference in the height of peaks corresponding to the Mg−anion and Mg−solvent interaction is significant for the N chelating solvents AN and DMA, which results in the formation of AGGs in solution. But unlike $Mg(TFSI)_2$, among O chelating solvents, the difference in peak height is large even for G1, G2, DMSO and THF which also results in the formation of AGGs. Only the higher order glymes, such as G4, can compete with BF_4^- in the interaction with Mg^{2+} which results in better dissociation of $Mg(BF_4)_2$ in G4 as compared to other solvents. The snapshots shown in Figure S10−S16 show significant cluster formation of $Mg(BF_4)_2$ in AN, DMA, G1 and THF solvents. For the $Mg(BH_4)_2$ salt we computed the RDF between Mg−H(BH_4), Mg−B(BH_4), Mg−N(AN, DMA), Mg−O(G1, G2, G4, DMSO, THF) and Mg−Mg (Figure S17−S23). In the solvation structure of $Mg(BH_4)_2$ the first peak is observed at 2 Å from Mg−H(BH_4) followed by a peak at 2.3 Å from Mg−B(BH_4). The sharper peak of Mg−H(BH_4) as compared to Mg−B(BH_4) indicates very strong bonding between Mg and H atoms of BH_4. Our previous work on $Mg(BH_4)_2$ in glymes, using both simulations and experiments, also suggests that Mg is covalently bonded with BH_4 anion through Mg−H bond.[70] Among glymes, the solvation improves with chain length from G1 to G4 which is also confirmed from our previous experimental work.[70] Similar to $Mg(TFSI)_2$ and $Mg(BF_4)_2$ the N chelating solvents show poor solvation. Among the 7 studied solvents, DMSO exhibits the best dissociating properties for $Mg(BH_4)_2$. For the three salts studied we observed a minima close to zero between the first and second solvation shells in RDF of Mg−anion and Mg−solvent indicating that Mg^{2+} forms a very well-defined and rigid first solvation shell.

Figure 4 shows the Mg−anion and Mg−solvent coordination numbers, obtained by integrating the RDF curve for the first solvation shell, for the seven solvents considered in this work. The coordination number of anions around Mg^{2+} is computed by integrating the first peak of RDF of Mg−N(TFSI), Mg−B(BF_4) and Mg−B(BH_4) in $Mg(TFSI)_2$, $Mg(BF_4)_2$ and $Mg(BH_4)_2$ respectively. The coordination number for solvents around Mg^{2+} is computed by integrating the first peak of RDF of Mg−N(AN), Mg−N(DMA), Mg−O(G1), Mg−O(G2), Mg−O-(G4), Mg−O(DMSO) and Mg−O(THF). For better solvation it is desirable to have higher coordination of Mg^{2+} with the solvent than the salt anion. The results shown in Figure 4 indicate that $Mg(TFSI)_2$ is most dissociated in DMSO and G4 and forms CIPs in G2 solvents. In DMSO and G4 the Mg^{2+} ions are ca. 6-fold coordinated by O-donors from DMSO, G4 and $TFSI^-$ is well-solvated. We observed formation of CIPs of Mg−TFSI with ca. 6-fold coordination by O-donors from G2 and one or more

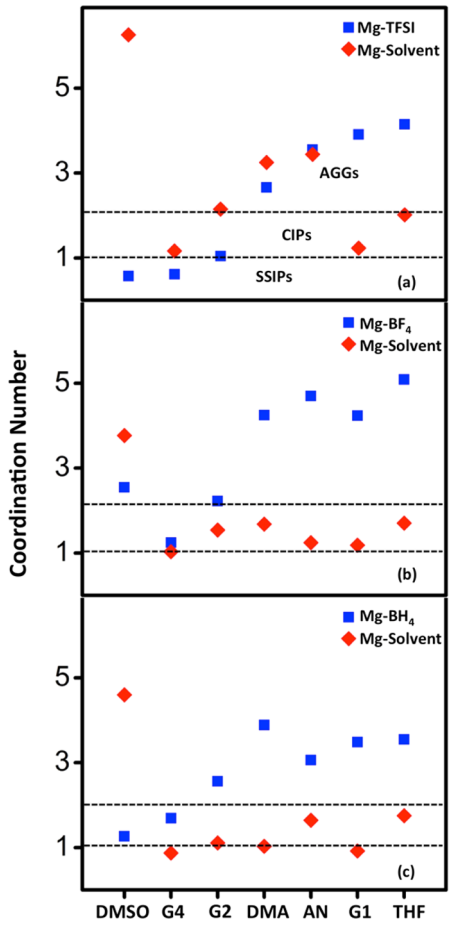

Figure 4. Coordination Number of (a) Mg−TFSI, (b) Mg−BF_4 and (c) Mg−BH_4 in 7 different solvents (shown on *x*-axis). The coordination numbers of Mg−TFSI, Mg−BF_4 and Mg−BH_4 are computed by integrating the first peak of RDF of Mg−N(TFSI), Mg−B(BF_4) and Mg−B(BH_4) respectively. The coordination number of the solvents around Mg^{2+} is computed by integrating the first peak of RDF of Mg−N(TFSI), Mg−B(BF_4), Mg−B(BH_4), Mg−N(AN), Mg−N(DMA), Mg−O(G1), Mg−O(G2), Mg−O(G4), Mg−O(DMSO) and Mg−O(THF).

oxygen atoms from $TFSI^-$. It was observed that the flexibility of glymes allows them to tightly wrap (chelate) around Mg^{2+} and adopt different conformations permitting better solvation. On the other hand, the high dielectric constant and small size of DMSO provide even better solvation. The RDFs and coordination number for $Mg(TFSI)_2$ in G2 agree very well with the experimental results obtained by X-ray scattering measurements and MD simulations in our previous work.[61] $Mg(TFSI)_2$ tends to form AGGs solvates in DMA, AN, G1 and THF. However, the protic nature of DMA allow it to provide better coordination with the anion, hence resulting in better solvation properties as compared to AN, G1 and THF. Figure S24 shows the RDFs and coordination number of $TFSI^-$ in different solvents. The coordination number of TFSI-DMA is larger than TFSI-AN, TFSI-G1 and TFSI-THF, which shows that even though DMA has a very low dielectric constant it can exhibit better dissociation of $Mg(TFSI)_2$ due to better coordination with $TFSI^-$. We observed very strong coordination between Mg^{2+} and BH_4^- as well as BF_4^-. $Mg(BF_4)_2$ tends to form CIPs in G4 and AGGs in all other solvents. Similarly, $Mg(BH_4)_2$ participates to form CIPs in DMSO and G4 and AGGs in all other solvents considered in this work, in agreement with the

DOI: 10.1021/jacs.5b01004
J. Am. Chem. Soc. XXXX, XXX, XXX−XXX

observed poor solubility of this salt. From the obtained information, we surmise that higher dissociation of Mg^{2+} and $TFSI^-$ as compared to BF_4^- and BH_4^- is due to delocalization of the negative charge, steric effect and large size of $TFSI^-$. It should be noted that DMSO performs very well in solvating $Mg(TFSI)_2$ and $Mg(BH_4)_2$ as compared to other solvents but $Mg(BF_4)_2$ is most dissociated in G4. Consistent with our predictions, previous experimental studies have confirmed better dissolution of Mg salts in DMSO as compared to AN and THF.[71] Interestingly, despite its high dielectric constant, AN shows poor solvation for most salts, which we speculate could be due to its weak coordination with anions, as anion solvation is mainly due to hydrogen bonding which is not observed in aprotic solvents such as AN.[54] Hence, the solvation structure depends on the properties of the anion, the solvent as well as the chain length and chelating properties of the solvating species. Finally, specifically for $Mg(TFSI)_2$ in G2, we performed a series of concentration dependent MD simulations which showed that CIPs are formed for salt concentrations at or above 0.4 M (Figure S25). We observed that the coordination number of Mg−TFSI increases and that of Mg−G2 decreases monotonically as a function of concentration. This could explain the experimental observations of different cathodic stability behavior for this salt as a function of concentration by Ha et al.[28]

In summary, from the solvation structures we observed a broad consistent ion pairing between the Mg cation and the anionic species indicating difficulty for most solvents to break the strong interaction between the salt cation and anion. Furthermore, the results show that, despite their low dielectric constant, glymes are powerful solvents, providing better dissociation of the Mg salts, due to the strong coordination between Mg and O of the glyme chain. Our previous study of $Mg(BH_4)_2$ in glymes using nuclear magnetic resonance (NMR), Fourier transform infrared spectroscopy (FTIR) and theoretical modeling show that the ionic association of Mg−BH_4 decreases with increase in chain length of glymes which in turn enhances the electrochemical performance of Mg batteries, adding further evidence to the importance of solvation for the electrochemical performance of the battery.[70] Finally, we emphasize that some of the low dielectric constant solvents with no functional groups such as G2, G4 provide better solvation to Mg salts as compared to high dielectric constant solvents such as AN and that the dissociation increases with the increase in O-donor denticity of glymes.

4. Dynamical Properties. Finally, we study the translational dynamics, which provide fundamental understanding of mass transport, conductivity and rheology of liquids, particularly highlighting the correlation between dynamics and solvation structure. Slow mass transport across the electrolyte at high concentration significantly affects the performance of batteries. Similar to the solvation structure, dynamics of ions also varies with concentration, as well as solvent and counterion chemistry. Previous experimental studies demonstrated the effect of salt concentration and slow dynamics of Mg electrolytes on electrochemical properties.[72] In Figure 5, we present the self-diffusion coefficient of Mg^{2+} and counteranion in (a) $Mg(TFSI)_2$, (b) $Mg(BF_4)_2$ and (c) $Mg(BH_4)_2$ in the considered solvents. We note that Mg^{2+} exhibit the slowest mobility in G4 and very fast mobility in high dielectric constant solvents such as AN and DMSO. For $Mg(TFSI)_2$ the dynamics of Mg^{2+} and $TFSI^-$ is fastest in AN followed by G1 and DMSO. Even though G1, G2 and G4 exhibit similar dielectric constants, $Mg(TFSI)_2$ tends to form SSIPs in G4, CIPs in G2 and AGGs in G1 and the mobility of Mg^{2+} ions is faster in G1 as compared to G4. Hence,

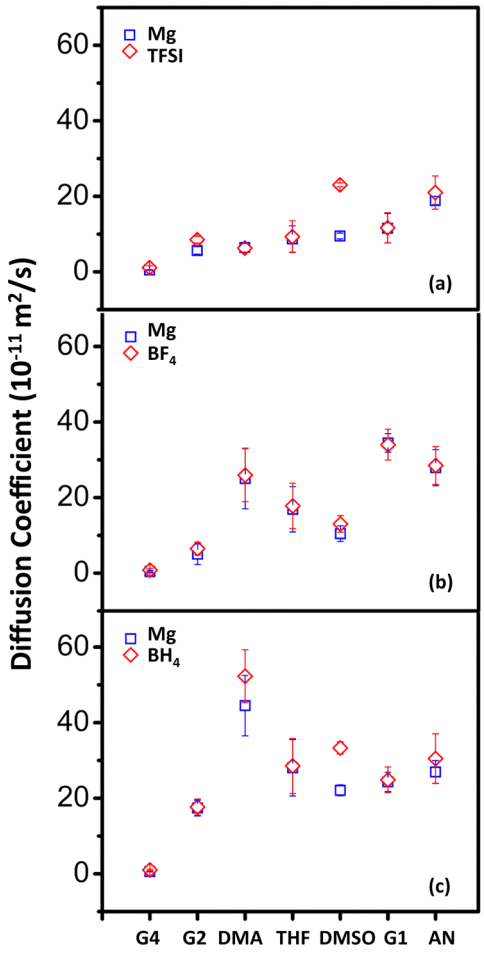

Figure 5. Self-diffusion coefficients of (a) Mg^{2+} and $TFSI^-$ (b) Mg^{2+} and BF_4^- and (c) Mg^{2+} and BH_4^- in 7 different solvents (shown on *x*-axis) displayed with error bars. An average error of ∼24% (with a maximum error of ∼50%) was estimated based on the difference of the diffusion coefficients obtained from fits over the two halves of the fit interval.

short chain ether solvents such as G1 could show better transport properties of Mg^{2+} ions as compared to G4 due to weaker solvation structure. The trends observed in glyme-based solvents are similar for all three salts ($Mg(TFSI)_2$, $Mg(BF_4)_2$ and $Mg(BH_4)_2$). The interaction between Mg^{2+} and O-donors of glymes is enhanced for longer-chain glymes, which improves the solubility of Mg salts but decreases the mobility of cation and anion in the solution. The results compliment the experimental results, where G2 provides better dissociation for $Mg(TFSI)_2$ and conversely, G1 provides better mobility of ions as compared to G2.[28] On the other hand, DMSO provides good solvating property as well as better mobility for both Mg^{2+} and $TFSI^-$. Hence the mobility of ions in the solution is also a function of the size of solvent molecules. For the range of salts considered, THF, a widely used solvent for Mg batteries, exhibits inferior solvation as well as moderate transport properties. Mobility of Mg^{2+} ions is faster for the $Mg(BH_4)_2$ salt as compared to $Mg(TFSI)_2$ and $Mg(BF_4)_2$ in most solvents except G1, where $Mg(BF_4)_2$ exhibits the fastest mobility. The bulky nature of $TFSI^-$ results in slower dynamics as compared to BH_4^- and BF_4^-anions. Although the large size and dispersed charge of $TFSI^-$ allows better solvation of Mg^{2+}, it also results in slower dynamics of Mg^{2+} in solution. The weak coordination strength of AN with Mg^{2+} and the high solvent dielectric constant help in improving the dynamics of

DOI: 10.1021/jacs.5b01004
J. Am. Chem. Soc. XXXX, XXX, XXX−XXX

both cation and anion. The calculated diffusion coefficients of Mg^{2+} in $Mg(TFSI)_2$/G2 are in good agreement with the experimental results measured by the chronocoulometry method (Figure S27). Figure S26 compares the self-diffusion coefficient of Mg^{2+} in $Mg(TFSI)_2$/G2, as a function of concentration, from simulations and experiments. The slower dynamics from simulations as compared to experiments is a common limitation of nonpolarizable force fields particularly for high viscosity liquids. However, previous work on carbonate electrolytes shows that the nonpolarizable force fields used in this work adequately reproduce the trends of diffusion coefficient as a function of concentration observed from experiments.,[73] as indeed is also found to be the case here (see Figure S26).[74]

In all systems studied the mobility of anions ($TFSI^-$, BF_4^-, BH_4^-) is similar or faster than Mg^{2+}, depending on the formation of ion pairs. The large difference in the dynamics of the cation and anion in the $Mg(TFSI)_2$/DMSO and $Mg(BH_4)_2$/DMSO solution is likely due to the strong interaction of DMSO with Mg^{2+} ions and thus resulting well-solvated salt components. Previous studies have shown that Mg electrolytes are found to exhibit moderate ionic conductivity and low transference number.[72] The inferior diffusion properties of Mg electrolytes observed in this work as compared to Li electrolytes ($1-3 \times 10^{-6}$ cm^2 s^{-1} in 1 M $LiPF_6$) could be attributed to the strong association of Mg^{2+} with anions found in the solvation structure of Mg electrolytes and will hence also show a marked dependence on the salt concentration and threshold for CIPs formation.[75]

CONCLUSION

By examining a matrix of salt and solvent combinations for potential Mg electrolytes, using combined MD and first-principles simulations, we find that Mg salts show a high tendency toward contact ion pair formation and aggregates in most organic solvents. This solvation structure is shown to impact not only the dynamics and charge transfer of the electrolyte, but also the stability of some anions. At Mg metal potentials, the ion pair undergoes reduction at the Mg cation center, which can activate the anion and can render it susceptible to decomposition. Under the operating conditions of electrochemical plating, this process will compete with the charge transfer mechanism where the Mg cation obtains a second electron and deposits on the Mg metal electrode surface. A few anions, such as BH_4^- and BF_4^-, are shown to be stable against Mg metal reduction, even in ion pair formation, in agreement with available experimental results. Importantly, we find that the $TFSI^-$ anion exhibits a rapid decomposition mechanism that is strongly dependent on the ion pair formation, which provides a possible explanation as to why $Mg(TFSI)_2$/glyme/diglyme shows conflicting evidence of stability against Mg metal potentials, particularly at different concentrations. The solvation of Mg electrolytes is better in oxygen donor solvents as compared to nitrogen donor solvents considered in this work. Furthermore, we observe that higher order glymes improves the solubility of Mg salts but reduces the dynamics of the ions in solution. Some widely used solvents such as tetrahydrofuran and acetonitrile exhibit poor solvating properties resulting in the formation of aggregates in solution, even at moderate concentrations. By examining the trends in solvation vs dielectric properties we confirm that the solvation of Mg salts is not directly correlated to the dielectric constant of solvents, but through a more complex dependence on the solvent molecular size, oxygen/nitrogen denticity and chelation. We hope this study contributes to an improved understanding of the impact of intermolecular interactions in Mg electrolytes on properties such as salt stability, dynamics and charge transfer toward the goal of rational design of multivalent electrolytes.

ASSOCIATED CONTENT

Supporting Information

Supporting figures and tables. This material is available free of charge via the Internet at http://pubs.acs.org.

AUTHOR INFORMATION

Corresponding Author

kapersson@lbl.gov

Author Contributions

§N.N.R. and X.Q. contributed equally.

Notes

The authors declare no competing financial interest.

ACKNOWLEDGMENTS

This work was supported as part of the Joint Center for Energy Storage Research (JCESR), an Energy Innovation Hub funded by the U.S. Department of Energy, under Contract No. DE-AC02-06CH11357. High performance computational resources for this research were provided by the National Energy Research Scientific Computing Center, which is supported by the Office of Science of the U.S. Department of Energy under Contract No. DE-AC02-05CH11231. The Materials Project (BES DOE Grant No. EDCBEE) is acknowledged for infrastructure and algorithmic support.

REFERENCES

(1) Whittingham, M. S.; Gamble, F. R. *Mater. Res. Bull.* **1975**, *10*, 363.
(2) Whittingham, M. S. *J. Electrochem. Soc.* **1975**, *122*, 526.
(3) Murphy, D.; Di Salvo, F.; Carides, J.; Waszczak, J. *Mater. Res. Bull.* **1978**, *13*, 1395.
(4) Nagaura, T.; Tozawa, K. *Prog. Batteries Sol. Cells* **1990**, *9*, 209.
(5) Tarascon, J. M.; Armand, M. *Nature* **2001**, *414*, 359.
(6) Saha, P.; Datta, M. K.; Velikokhatnyi, O. I.; Manivannan, A.; Alman, D.; Kumta, P. N. *Prog. Mater. Sci.* **2014**, *66*, 1.
(7) Brown, O.; McIntyre, R. *Electrochim. Acta* **1985**, *30*, 627.
(8) Lu, Z.; Schechter, A.; Moshkovich, M.; Aurbach, D. *J. Electroanal. Chem.* **1999**, *466*, 203.
(9) Peled, E.; Straze, H. *J. Electrochem. Soc.* **1977**, *124*, 1030.
(10) Liebenow, C. *J. Appl. Electrochem.* **1997**, *27*, 221.
(11) Liebenow, C.; Yang, Z.; Lobitz, P. *Electrochem. Commun.* **2000**, *2*, 641.
(12) Brenner, A. *J. Electrochem. Soc.* **1971**, *118*, 99.
(13) Gregory, T. D.; Hoffman, R. J.; Winterton, R. C. *J. Electrochem. Soc.* **1990**, *137*, 775.
(14) Aurbach, D.; Lu, Z.; Schechter, A.; Gofer, Y.; Gizbar, H.; Turgeman, R.; Cohen, Y.; Moshkovich, M.; Levi, E. *Nature* **2000**, *407*, 724.
(15) Aurbach, D.; Suresh, G. S.; Levi, E.; Mitelman, A.; Mizrahi, O.; Chusid, O.; Brunelli, M. *Adv. Mater.* **2007**, *19*, 4260.
(16) Doe, R. E.; Han, R.; Hwang, J.; Gmitter, A. J.; Shterenberg, I.; Yoo, H. D.; Pour, N.; Aurbach, D. *Chem. Commun.* **2014**, *50*, 243.
(17) Muldoon, J.; Bucur, C. B.; Oliver, A. G.; Sugimoto, T.; Matsui, M.; Kim, H. S.; Allred, G. D.; Zajicek, J.; Kotani, Y. *Energy Environ. Sci.* **2012**, *5*, 5941.
(18) Kim, H. S.; Arthur, T. S.; Allred, G. D.; Zajicek, J.; Newman, J. G.; Rodnyansky, A. E.; Oliver, A. G.; Boggess, W. C.; Muldoon, J. *Nat. Commun.* **2011**, *2*, 427.
(19) Shao, Y.; Liu, T.; Li, G.; Gu, M.; Nie, Z.; Engelhard, M.; Xiao, J.; Lv, D.; Wang, C.; Zhang, J.-G. *Sci. Rep.* **2013**, DOI: 10.1038/srep03130.

DOI: 10.1021/jacs.5b01004
J. Am. Chem. Soc. XXXX, XXX, XXX−XXX

(20) Geoffroy, I.; Willmann, P.; Mesfar, K.; Carré, B.; Lemordant, D. *Electrochim. Acta* **2000**, *45*, 2019.
(21) Tobishima, S.; Morimoto, H.; Aoki, M.; Saito, Y.; Inose, T.; Fukumoto, T.; Kuryu, T. *Electrochim. Acta* **2004**, *49*, 979.
(22) Shterenberg, I.; Salama, M.; Gofer, Y.; Levi, E.; Aurbach, D. *MRS Bull.* **2014**, *39*, 453.
(23) Mohtadi, R.; Matsui, M.; Arthur, T. S.; Hwang, S.-J. *Angew. Chem., Int. Ed.* **2012**, *51*, 9780.
(24) Shao, Y.; Gu, M.; Li, X.; Nie, Z.; Zuo, P.; Li, G.; Liu, T.; Xiao, J.; Cheng, Y.; Wang, C.; Zhang, J.-G.; Liu, J. *Nano Lett.* **2013**, *14*, 255.
(25) Arthur, T. S.; Singh, N.; Matsui, M. *Electrochem. Commun.* **2012**, *16*, 103.
(26) Tran, T. T.; Lamanna, W.; Obrovac, M. *J. Electrochem. Soc.* **2012**, *159*, A2005.
(27) Pour, N.; Gofer, Y.; Major, D. T.; Aurbach, D. *J. Am. Chem. Soc.* **2011**, *133*, 6270.
(28) Ha, S.-Y.; Lee, Y.-W.; Woo, S. W.; Koo, B.; Kim, J.-S.; Cho, J.; Lee, K. T.; Choi, N.-S. *ACS Appl. Mater. Interfaces* **2014**, *6*, 4063.
(29) Lossius, L. P.; Emmenegger, F. *Electrochim. Acta* **1996**, *41*, 445.
(30) Szwarc, M. *Pure Appl. Chem.* **1976**, *48*, 247.
(31) Giffin, G. A.; Moretti, A.; Jeong, S.; Passerini, S. *J. Phys. Chem. C* **2014**, *118*, 9966.
(32) Minofar, B.; Vácha, R.; Wahab, A.; Mahiuddin, S.; Kunz, W.; Jungwirth, P. *J. Phys. Chem. B* **2006**, *110*, 15939.
(33) Aresta, M.; Quaranta, E.; Tommasi, I.; Derien, S.; Dunach, E. *Organometallics* **1995**, *14*, 3349.
(34) Hipps, K.; Aplin, A. *J. Phys. Chem.* **1985**, *89*, 5459.
(35) Xu, W.; Angell, C. A. *Electrochem. Solid-State Lett.* **2001**, DOI: 10.1149/1.1344281.
(36) Bjerrum, N. *K. Dan. Vidensk. Selsk.* **1926**, *7*, 9.
(37) Ong, S. P.; Andreussi, O.; Wu, Y.; Marzari, N.; Ceder, G. *Chem. Mater.* **2011**, *23*, 2979.
(38) Krylov, A. I.; Gill, P. M. *Wiley Interdiscip. Rev.: Comput. Mol. Sci.* **2013**, *3*, 317.
(39) Shao, Y.; Gan, Z.; Epifanovsky, E.; Gilbert, A. T.; Wormit, M.; Kussmann, J.; Lange, A. W.; Behn, A.; Deng, J.; Feng, X. *Mol. Phys.* **2014**, DOI: 10.1080/00268976.2014.952696.
(40) Becke, A. D. *J. Chem. Phys.* **1993**, *98*, 1372.
(41) Tomasi, J.; Mennucci, B.; Cances, E. *J. Mol. Struct.: THEOCHEM* **1999**, *464*, 211.
(42) Rappe, A. K.; Casewit, C. J.; Colwell, K. S.; Goddard, W. A.; Skiff, W. M. *J. Am. Chem. Soc.* **1992**, *114*, 10024.
(43) Cheng, L.; Assary, R. S.; Qu, X.; Jain, A.; Ong, S. P.; Rajput, N. N.; Persson, K.; Curtiss, L. A. *J. Phys. Chem. Lett.* **2014**, *6*, 283.
(44) Xiaohui, Q. A. J.; Rajput, N. N.; Zhang, Y.; Ong, S. P.; Brafman, M.; Cheng, L.; Maginn, E.; Curtiss, L. A.; Persson, K. A., unpublished.
(45) Hobza, P.; Müller-Dethlefs, K. *Non-Covalent Interactions: Theory and Experiment*; Royal Society of Chemistry: Cambridge, U.K., 2010.
(46) Pronk, S.; Páll, S.; Schulz, R.; Larsson, P.; Bjelkmar, P.; Apostolov, R.; Shirts, M. R.; Smith, J. C.; Kasson, P. M.; van der Spoel, D. *Bioinformatics* **2013**, btt055.
(47) Wang, J.; Wolf, R. M.; Caldwell, J. W.; Kollman, P. A.; Case, D. A. *J. Comput. Chem.* **2004**, *25*, 1157.
(48) Berendsen, H. J.; Postma, J. P. M.; van Gunsteren, W. F.; DiNola, A.; Haak, J. *J. Chem. Phys.* **1984**, *81*, 3684.
(49) Bussi, G.; Donadio, D.; Parrinello, M. *J. Chem. Phys.* **2007**, *126*, 014101.
(50) Bussi, G.; Zykova-Timan, T.; Parrinello, M. *J. Chem. Phys.* **2009**, *130*, 074101.
(51) Borodin, O.; Behl, W.; Jow, T. R. *J. Phys. Chem. C* **2013**, *117*, 8661.
(52) Aurbach, D.; Gizbar, H.; Schechter, A.; Chusid, O.; Gottlieb, H. E.; Gofer, Y.; Goldberg, I. *J. Electrochem. Soc.* **2002**, *149*, A115.
(53) Henderson, W. A. *J. Phys. Chem. B* **2006**, *110*, 13177.
(54) Seo, D. M.; Borodin, O.; Han, S.-D.; Boyle, P. D.; Henderson, W. A. *J. Electrochem. Soc.* **2012**, *159*, A1489.
(55) Apelblat, A. *J. Solution Chem.* **2011**, *40*, 1234.
(56) Bakker, A.; Gejji, S.; Lindgren, J.; Hermansson, K.; Probst, M. M. *Polymer* **1995**, *36*, 4371.
(57) Pye, C. C.; Rudolph, W. W. *J. Phys. Chem. A* **1998**, *102*, 9933.
(58) Wahab, A.; Mahiuddin, S.; Hefter, G.; Kunz, W.; Minofar, B.; Jungwirth, P. *J. Phys. Chem. B* **2005**, *109*, 24108.
(59) Nakayama, Y.; Kudo, Y.; Oki, H.; Yamamoto, K.; Kitajima, Y.; Noda, K. *J. Electrochem. Soc.* **2008**, *155*, A754.
(60) Mizrahi, O.; Amir, N.; Pollak, E.; Chusid, O.; Marks, V.; Gottlieb, H.; Larush, L.; Zinigrad, E.; Aurbach, D. *J. Electrochem. Soc.* **2008**, *155*, A103.
(61) Lapidus, S. H.; Rajput, N. N.; Qu, X.; Chapman, K. W.; Persson, K. A.; Chupas, P. J. *Phys. Chem. Chem. Phys.* **2014**, *16*, 21941.
(62) Marcus, R. A. *J. Phys. Chem. B* **1998**, *102*, 10071.
(63) Vakarin, E. V.; Holovko, M. F.; Piotrowiak, P. *Chem. Phys. Lett.* **2002**, *363*, 7.
(64) Dupon, R.; Papke, B. L.; Ratner, M. A.; Whitmore, D. H.; Shriver, D. F. *J. Am. Chem. Soc.* **1982**, *104*, 6247.
(65) Papke, B. L.; Dupon, R.; Ratner, M. A.; Shriver, D. F. *Solid State Ionics* **1981**, *5*, 685.
(66) McOwen, D. W.; Seo, D. M.; Borodin, O.; Vatamanu, J.; Boyle, P. D.; Henderson, W. A. *Energy Environ. Sci.* **2014**, *7*, 416.
(67) Hu, J.; Long, G.; Liu, S.; Li, G.; Gao, X. *Chem. Commun.* **2014**, *50*, 14647.
(68) Kalhoff, J.; Bresser, D.; Bolloli, M.; Alloin, F.; Sanchez, J. Y.; Passerini, S. *ChemSusChem* **2014**, *7*, 2939.
(69) Howlett, P. C.; Izgorodina, E. I.; Forsyth, M.; Macfarlane, D. R. *Z. Phys. Chem.* **2006**, *220*, 1483.
(70) Shao, Y.; Rajput, N. N.; Hu, J.; Hu, M.; Liu, T.; Wei, Z.; Gu, M.; Deng, X.; Xu, S.; Han, K. S. *Nano Energy* **2014**, DOI: 10.1016/j.nanoen.2014.12.028.
(71) Giraudet, J.; Claves, D.; Guérin, K.; Dubois, M.; Houdayer, A.; Masin, F.; Hamwi, A. *J. Power Sources* **2007**, *173*, 592.
(72) Benmayza, A.; Ramanathan, M.; Arthur, T. S.; Matsui, M.; Mizuno, F.; Guo, J.; Glans, P.-A.; Prakash, J. *J. Phys. Chem. C* **2013**, *117*, 26881.
(73) Han, K. S.; Rajput, N. N.; Wei, X.; Wang, W.; Hu, J. Z.; Persson, K. A.; Mueller, K. T. *J. Chem. Phys.* **2014**, *141*, 104509.
(74) Maginn, E. J. *J. Phys.: Condens. Matter* **2009**, *21*, 373101.
(75) Stewart, S. G.; Newman, J. *J. Electrochem. Soc.* **2008**, *155*, F13.

DOI: 10.1021/jacs.5b01004
J. Am. Chem. Soc. XXXX, XXX, XXX−XXX